Atmospheric Environment 186 (2018) 102–112

Contents lists available at ScienceDirect

Atmospheric Environment

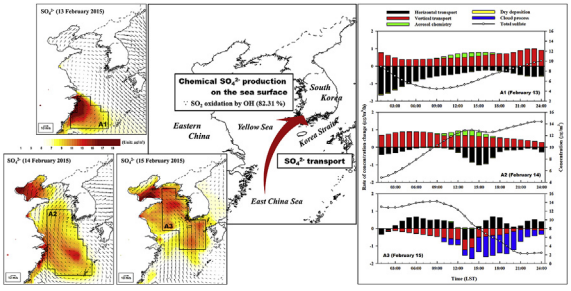
journal homepage: www.elsevier.com/locate/atmosenv

Behavior of sulfate on the sea surface during its transport from Eastern China to South Korea

Wonbae Jeon[a,b], Yunsoo Choi[b], Jeonghyeok Mun[c], Soon-Hwan Lee[d], Hyun-Jeong Choi[e], Jung-Woo Yoo[c], Hyo-Jung Lee[a], Hwa Woon Lee[f,*]

[a] Institute of Environmental Studies, Pusan National University, Busan 46241, South Korea
[b] Department of Earth and Atmospheric Sciences, University of Houston, Houston, TX 77204, USA
[c] Division of Earth Environmental System, Pusan National University, Busan 46241, South Korea
[d] Department of Earth Science Education, Pusan National University, Busan 46241, South Korea
[e] Department of Physics and Earth Science, Korea Science Academy of KAIST, Busan 47162, South Korea
[f] Department of Atmospheric Sciences, Pusan National University, Busan 46241, South Korea

GRAPHICAL ABSTRACT



ARTICLE INFO

Keywords:
Sulfate
Long-range transport
CMAQ
Process analysis

ABSTRACT

This study investigates the production/loss of sulfate on the sea surface during its transport from Eastern China to South Korea (Korea). We use the Community Multi-scale Air Quality (CMAQ) model to simulate sulfate concentrations in February 2015 and to examine the changes in them. Results of the CMAQ simulation show high sulfate concentrations over the sea surface areas between Eastern China and Korea despite nearly zero emissions. Their concentrations gradually increased (from 0.371 to 0.581μg/m_3/h) as they passed through the East China Sea, the Yellow Sea, and the Korea Strait. The results from a quantitative analysis using the integrated process rate (IPR) in CMAQ suggest that increasing sulfate concentrations during the transport was mainly attributable to chemical sulfate productions by the aerosol process (up to 0.866μg/m^3/h) and vertical transport (up to 0.994μg/m^3/h) of chemically produced sulfate, resulting from vertical momentum transport caused by vertical wind shear and temperature gradient. The results of the sulfur tracking model (STM) in CMAQ verify that the OH + SO_2 → H_2SO_4 + HO_2 reaction was the largest contributor (82.31%) to the production of sulfate over the sea surface areas during its transport. Surplus SO_2 in the transporting plume reacted to abundant OH over the sea surface, formed H_2SO_4, and contributed to the consequently increased sulfate concentrations. The observed sulfate data in Korea confirm that sulfate concentrations over the sea surface areas enhanced sulfate concentrations in Korea (from 12.27 to 13.74μg/m^3). The sulfate, however, was not directly transported from upwind regions but chemically produced during the transport. The results of several sensitivity simulations with

* Corresponding author.
E-mail address: hwlee@pusan.ac.kr (H.W. Lee).

https://doi.org/10.1016/j.atmosenv.2018.05.017
Received 1 February 2018; Received in revised form 8 May 2018; Accepted 10 May 2018
Available online 11 May 2018
1352-2310/ © 2018 Elsevier Ltd. All rights reserved.

varied meteorology revealed that the changes in chemical sulfate production rates during the transport of sulfate were mainly affected by temperature.

1. Introduction

A major inorganic species in particulate matter (PM), sulfate, affects the radiative balance of the Earth and exerts adverse effects on human health (Son et al., 2012; Lin et al., 2017). Sulfate is primarily produced through the gas-phase oxidation and aqueous reactions of sulfur dioxide (SO_2) (Seinfeld and Pandis, 2006; Park et al., 2016). SO_2 is one of the major precursors of sulfate emitted from the combustion of fossil fuel (Kim et al., 2016; Paulot et al., 2017). The largest contributor to global anthropogenic SO_2 emissions is China (Li et al., 2017). These emissions, which are often transported to downwind regions such as South Korea (Korea, hereafter), Japan, and the western United States (Itahashi et al., 2012; Lin et al., 2017), leading to high sulfate formation in these regions. In particular, air pollution in Korea is strongly influenced by long-range transported foreign emissions from the upwind countries (e.g., China and Mongolia) because of the source-receptor relationship between the countries (Han et al., 2005, 2006; Kim et al., 2010; Choi et al., 2014; Jeon et al., 2014a). Kim et al. (2017a) reported that over 70% of PM in Korea during the cold season (December–March) in 2014 was attributable to Chinese and Mongolian emissions. Also, several other studies (Park et al., 2016; Shin et al., 2016; Kim et al., 2017b) reported noticeably large sulfate concentration in Korea during the period of long-range transport from upwind source regions. As sulfate, during periods of high PM concentrations, is a substantial contributor of PM constituents in Korea, enhancing our understanding of the mechanism of high PM formation in Korea demands a more comprehensive knowledge of sulfate transport (He et al., 2014; Huang et al., 2014).

According to several previous studies, an understanding of the chemical processes that take place during the transport of pollutants from a source to a receptor region is crucial to identifying the exact mechanism of the local air pollution phenomenon (Heo et al., 2009; Jeon et al., 2012, 2014b; 2018; Park et al., 2016). Since long-range transported sulfate and its precursors from China to Korea frequently results in high sulfate concentrations in Korea (Itahashi et al., 2012; Kim et al., 2016), investigating their behavior during the transport could help us identify the mechanism that contributes to high PM in Korea (Shin et al., 2016; Kim et al., 2017b).

Despite the previous studies that have examined sulfate transport, the detailed behavior of sulfate in transporting PM plumes is not fully understood. Although several studies (Heo et al., 2009; Zhang et al., 2012; Choi et al., 2013; Kim et al., 2017a, 2017b) have investigated the source apportionment of PM in Korea, few studies have quantitatively examined chemical changes in sulfate transport. Thus, this study investigates the chemistry associated with sulfate production and loss during its transport from Eastern China to Korea. As highly polluted air over Eastern China frequently passes over sea surface areas (e.g., the East China Sea and the Yellow Sea) before reaching Korea (Heo et al., 2009; Kim et al., 2017a), we examine chemical changes in sulfate on the sea surface. We use the Community Multi-scale Air Quality (CMAQ) (Byun and Schere, 2006) in simulations of sulfate concentrations in February 2015, from which our modeling system reasonably reproduced PM in Korea (Jeon et al., 2016). To evaluate the performance of the CMAQ simulations, we compare the results with corresponding in-situ measurements and investigate the feature of sulfate transport from Eastern China to Korea. Here, we employ the integrated process rate (IPR) (Gipson and Young, 1999) and the sulfur tracking model in

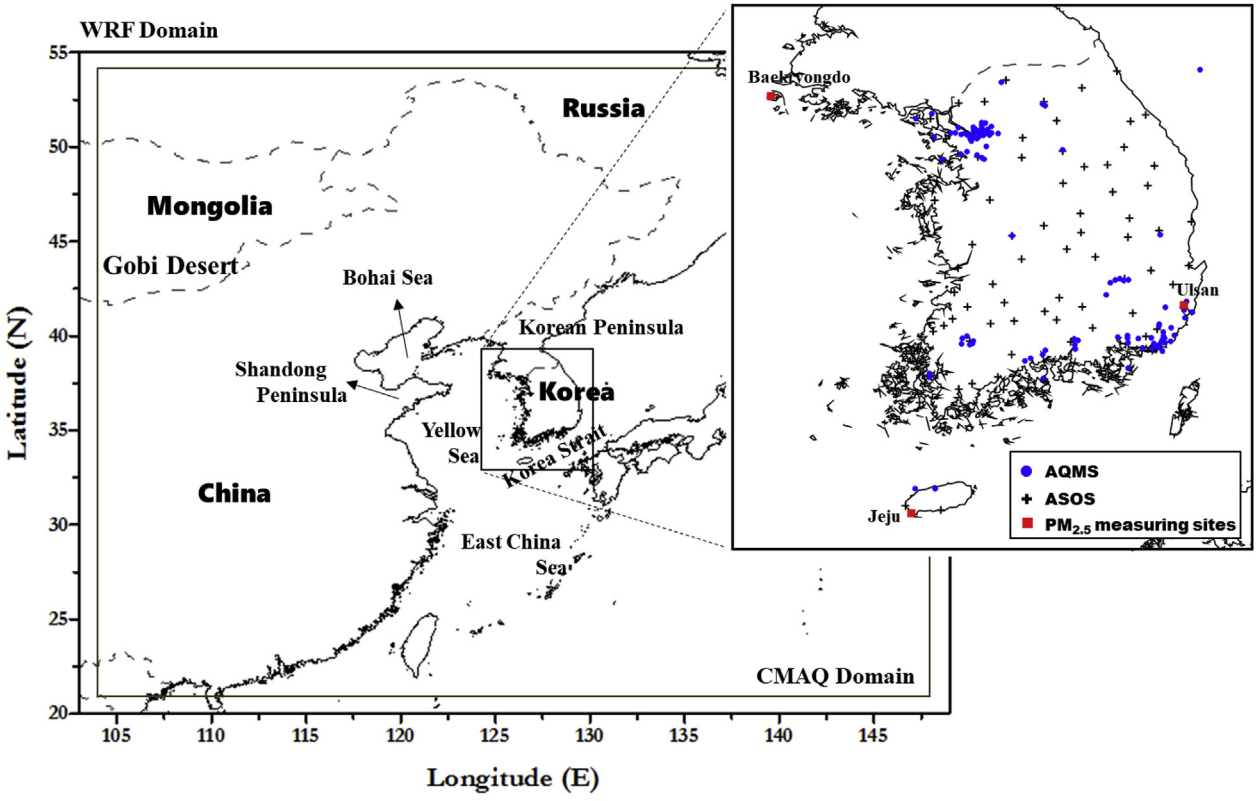


Fig. 1. Domains for WRF and CMAQ modeling, and the detailed topographic features in the vicinity of Korea. The right panel presents the locations of 75 ASOS, 106 AQMS, and 3 $PM_{2.5}$ measuring sites used in this study.

CMAQ (STM, hereafter) to quantitatively analyze chemical changes that occur during the transport of sulfate over the sea surface. Ultimately, we will identify the mechanism of high sulfate transport in Korea during the period of long-range transport from Eastern China to Korea.

2. Methodology

2.1. Modeling system and data

This study applies the United States Environmental Protection Agency (USEPA)'s CMAQ (v5.0.2) model. We configured the CMAQ domain, covering Northeast Asia that includes China, Korea, and Japan (Fig. 1), with a grid resolution of 15 km (267 × 218) and 27 vertical layers extending from the surface to 100 hPa. Carbon Bond 5 (CB05; Yarwood et al., 2005) and AERO6 (Nolte et al., 2015) were used for the gas-phase and aerosol chemical mechanisms. We acquired anthropogenic emissions for the CMAQ domain from the MIX emissions inventory in 2010 (Jeon et al., 2016; Kim et al., 2017a; Li et al., 2017; Souri et al., 2017) (Fig. S1). The inventory contains gridded (0.25° × 0.25°) emissions information for black carbon (BC), carbon monoxide (CO), carbon dioxide (CO_2), niterogen oxide (NO_x), ammonia (NH_3), organic carbon (OC), particulate matter ($PM_{2.5}$ and PM_{10}), SO_2, and non-methane volatile organic compounds (NMVOC). The biogenic emissions for the CMAQ domain were prepared by the Model of Emissions of Gases and Aerosols from Nature (MEGAN, v2.1) (Guenther et al., 2012). We obtained the meteorology for the CMAQ simulation from a Weather Research and Forecast (WRF, v3.7) (Skamarock et al., 2008) simulation, whose initial and boundary conditions came from the 1° × 1° Final Operational Global Analysis (FNL) data of the National Centers for Environmental Prediction (NCEP). WSM 3-class simple ice microphysics scheme, RRTM long-wave radiation scheme, Dudhia short-wave radiation scheme, Monin-Obukhov (Janic Eta) surface layer scheme, Unified Noah land-surface scheme, YSU PBL scheme, and Kain-Fritsch (new Eta) scheme were used for the WRF simulation. To improve the accuracy of the meteorology, we adopted optimized grid analysis nudging options reported by Jeon et al. (2015) and Souri et al. (2017). The Meteorology Chemistry Interface Processor (MCIP, v4.1) was used to provide the CMAQ-ready meteorology from the WRF simulation. The period for the WRF and CMAQ simulations was January 21 to February 28, 2015 (the first ten days for spin-up), previously simulated and comprehensively evaluated by a PM_{10} modeling study (Jeon et al., 2016). The detailed options used for the WRF and CMAQ simulations are listed in Tables S1 and S2.

2.2. IPR and STM

In this study, we employed the IPR module (in the CMAQ model), used for some researchers in their air quality studies (Li et al., 2014; Fan et al., 2015; Pan et al., 2015, 2017; Jeon et al., 2018). The module provides quantified contributions of individual processes (e.g., transport, chemistry, emissions, deposition, cloud process) to pollutant concentrations. We used the IPR to calculate the respective contributions of horizontal/vertical transport, gas- and aqueous-phase chemistry, the cloud process, dry deposition, and emissions to simulated sulfate concentrations. In addition, this study applied the STM, which tracked the budget of simulated sulfate concentration. It quantifies the contributions of individual chemical reactions, direct emissions, and initial and boundary conditions to the total sulfate production. It works with the standard CMAQ model and requires no additional input data. Table 1 summarizes the respective contributors to sulfate production calculated by the STM.

2.3. In-situ measurements

We used surface observational data from the air quality monitoring station (AQMS) network, operated by the National Institute of Environmental Research (NIER) in Korea. The network measures real-time air pollutant concentrations and provides hourly concentrations for CO, NO_2, O_3, $PM_{2.5}$, PM_{10}, and SO_2. We obtained meteorological data from the Automated Surface Observing System (ASOS) network, operated by the Korea Meteorological Administration (KMA) and gathered the measured surface temperature, the wind speed, and $PM_{2.5}$ data for the episode period of this study (February 2015) from 75 ASOS and 106 AQMS sites (Fig. 1) to evaluate the results from WRF and CMAQ simulations. To further evaluate the accuracy of the CMAQ simulation, we acquired observed hourly $PM_{2.5}$ speciation data (i.e., sulfate, nitrate, ammonium, OC, and elemental carbon (EC)) from three observation sites in Korea (Fig. 1).

2.4. Statistical parameters

To evaluate model performance, we used several statistical parameters such as the index of agreement (IOA), the mean bias error (MBE), the normalized root mean square error (NRMSE), and the mean fractional bias (MFB), all of which are defined as follows:

$$\mathrm{IOA} = 1 - \frac{\sum_{i=1}^{N}(P_i - O_i)^2}{\sum_{i=1}^{N}(|P_i - \overline{P}| + |O_i - \overline{O}|)^2}$$

$$\mathrm{MBE} = \frac{\sum_{i=1}^{N}(P_i - O_i)}{N}$$

$$\mathrm{NRMSE} = \frac{100}{O_{i,\ max} - O_{i,min}}\sqrt{\frac{\sum_{i=1}^{N}(P_i - O_i)^2}{N}}$$

$$\mathrm{MFB} = \frac{2}{N}\sum_{i=1}^{N}\frac{P_i - O_i}{P_i + O_i}$$

where N is the number of data points and P_i and O_i denote CMAQ-simulated and observed concentrations, respectively. With regard to the MFB, we used the performance goals and criteria proposed by Boylan and Russell (2006) to determine if our CMAQ simulation meets the reference values defined as follows:

$$|\mathrm{MFB\ (goals)}| \le 1.7e^{-2\overline{C}} + 0.3$$

$$|\mathrm{MFB\ (criteria)}| \le 1.4e^{-2\overline{C}} + 0.6$$

where $\overline{C}$ is $(\overline{P} + \overline{O})/2$, and $\overline{P}$ and $\overline{O}$ are the mean CMAQ-simulated and observed values, respectively.

3. Results and discussion

3.1. Evaluation of simulated concentrations of $PM_{2.5}$ constituents

As mentioned in Section 2.1, Jeon et al. (2016) simulated PM_{10} concentrations over Northeast Asia in February 2015 using the same modeling system used in this study and evaluated the model performance. They reported that CMAQ reasonably reproduced variations in PM_{10} in February 2015, except for the period of the Asian dust events (22–24 February). To validate these findings, we further evaluated the simulated $PM_{2.5}$ and each component (i.e., sulfate, nitrate, ammonium,

Table 1
Individual chemical reactions and factors contributing to sulfate production appearing in the STM. "MHP" and "PAA" denote methyl hydrogen peroxide and peroxyacetic acid, respectively.

Individual contributors to sulfate production	
[1] $OH + SO_2 \rightarrow H_2SO_4 + HO_2$	[2] $H_2O_2 + S(IV) \rightarrow S(VI) + H_2O$
[3] $O_3 + S(IV) \rightarrow S(VI) + O_2$	[4] $O_2 + S(IV) \rightarrow S(VI)$
[5] MHP + S(IV) → S(VI)	[6] PAA + S(IV) → S(VI)
[7] Emissions	[8] Initial and boundary conditions

OC, and EC), which the previous study had not done. As seen in Fig. 2, the WRF-simulated temperature was close to observations with high IOA (0.91) and low NRMSE (7.58%) and MBE (−1.29 °C). The simulated wind speed also closely agreed with the observations (IOA: 0.78, NRMSE: 10.68%, MBE: 1.29 m/s), indicating the reasonable accuracy of the WRF-simulated meteorology.

The CMAQ-simulated $PM_{2.5}$ closely matched corresponding observations as shown in Fig. 3-(a). CMAQ reasonably reproduced temporal variations in $PM_{2.5}$ (IOA: 0.75), but slightly underestimated $PM_{2.5}$ concentration (NRMSE: 10.86%, MBE: −4.30μg/m^3), likely due to the underestimated sulfate and OC, which accounted for the large portions of total $PM_{2.5}$ in Korea; sulfate 18.62% and OC 15.70% (Fig. S2). Unlike sulfate and OC, nitrate was overestimated, and ammonia and EC showed reasonable agreement with observations. The underestimation of sulfate and overestimation of nitrate are well-known issues in PM modeling in East Asia (Park and Kim, 2014; Ghim et al., 2017), attributable to uncertainties in emissions and inaccuracies of meteorology (e.g., Jeon et al., 2015; Chang et al., 2016). According to previous studies (Krotkov et al., 2016; van der A et al., 2017; Itahashi et al., 2018), the amount of SO_2 emissions over China indicates a decreasing trend after 2010, revealing the discrepancy of emissions between the two years (2010 and 2015). Since we used 2010 emissions data for the simulation in February 2015, the uncertainty in emissions might have caused the model-measurement error in this study.

The calculated MFB for $PM_{2.5}$, sulfate, nitrate, ammonium, OC, and EC were 0.40, −0.80, 0.70, 0.10, −1.10, and −0.10, respectively (Fig. 4). These results are similar to those found by a previous study (Ghim et al., 2017). All of the MFB values, except for that of OC, met the performance criteria proposed by Boylan and Russell (2006). Thus, we conclude that the simulation results are reliable and acceptable for application of the standard model, which allows for the underestimation of OC.

3.2. Features of simulated $PM_{2.5}$, sulfate, nitrate, and ammonium

We analyzed the transporting pathways of the high $PM_{2.5}$ plume in the modeling domain (Fig. 1) during the entire period of the CMAQ simulation and selected a partial period for intensive analysis on sulfate changes. On 13–15 February 2015, high $PM_{2.5}$ plumes over Eastern China and the East China Sea were transported to the Shandong Peninsula, the Bohai Sea, the Yellow Sea, and the Korean Peninsula (Fig. S3). During this period, the plumes notably passed over the East China Sea, the Yellow Sea, and the Korea Strait before reaching Korea. Therefore, we selected the three days (13–15 February 2015) as the partial period to further investigate the transporting features of the simulated sulfate.

Fig. 5 indicates the averaged concentrations of sulfate, nitrate, and ammonium around the Yellow Sea on 13–15 February 2015. Because of their dense emissions, their peaks equally appeared in Eastern China (Li et al., 2017). Interestingly, sulfate concentrations over the Yellow Sea and some areas of the East China Sea and the Korea Strait (Fig. 6) were noticeably high despite an absence of anthropogenic emissions, implying that sulfate featured a unique horizontal distribution compared to those of nitrate (Fig. S4) and ammonium (Fig. S5). To clarify the high sulfate concentration over the sea surface, we analyzed the variation of sulfate distribution around the Yellow Sea over time. At 00:00 LST on 13 February, a high concentration of sulfate appeared in the East China Sea and gradually moved to the west and north along with the wind blowing clockwise, which was caused by high pressure centered in the Yellow Sea. The high concentrations of sulfate continued to move and spread out over the Yellow Sea, some reaching the southwestern part of the Korean Peninsula at 00:00 LST on 15 February. It is worth noting that the sulfate concentration gradually increased during its transport from the East China Sea to Korea and was higher in the vicinity of Korea than it was near the East China Sea on 15 February.

3.3. Process analysis of the simulated sulfate concentration

As described in the previous section, sulfate was transported from the East China Sea to Korea on 13–15 February 2015, and its concentration increased. To quantitatively investigate the mechanism that led to the increase in sulfate concentrations over the sea surface areas (i.e., East China Sea, the Yellow Sea, and the Korea Strait), we conducted process analysis using the IPR. In the analysis, we separated the sea surface areas between Eastern China and Korea into three sub-areas, shown in Fig. 7. The areas present the locations of the transporting sulfate stayed on 13 (A1), 14 (A2), and 15 (A3) February, respectively. To determine the locations, we averaged the sulfate concentrations in

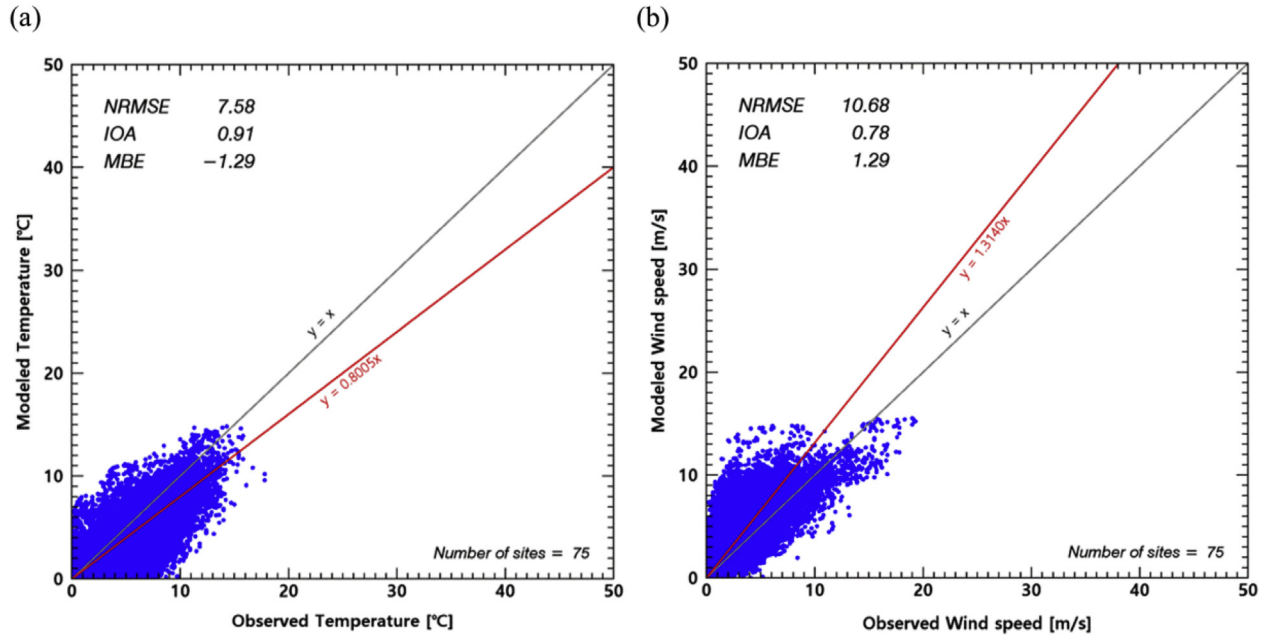


Fig. 2. Comparisons between the WRF-simulated (a) temperature, (b) wind speed, and corresponding observations (Fig. 1) during the entire period of simulation (February 2015).

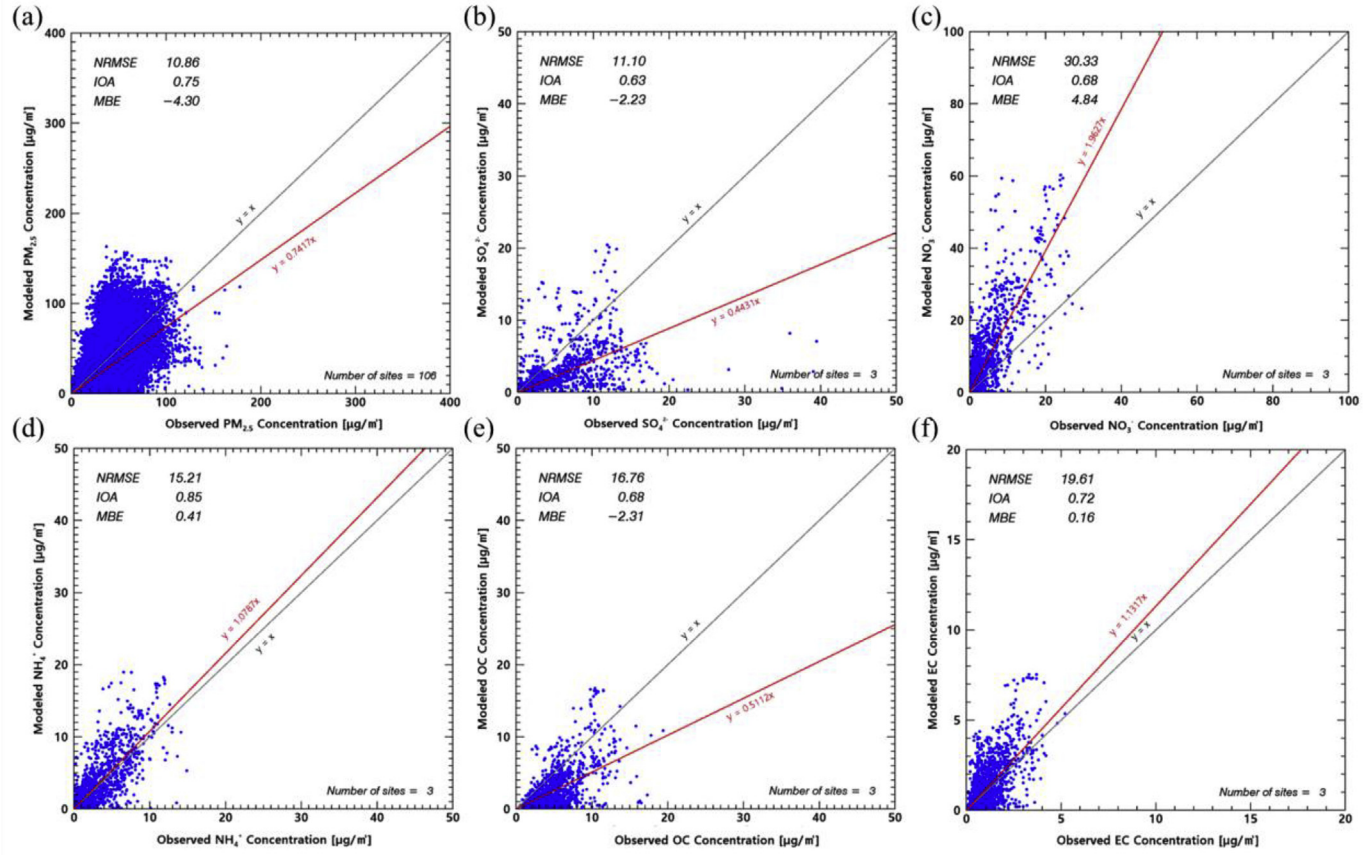


Fig. 3. Comparisons between the CMAQ-simulated (a) $PM_{2.5}$, (b) sulfate (SO_4^{2-}), (c) nitrate (NO_3^-), (d) ammonium (NH_4^+), (e) OC, and (f) EC, and corresponding observations (Fig. 1) during the entire period of simulation (February 2015).

the planetary boundary layer (PBL) height on these three days.

3.3.1. Sulfate changes in the early stage of transport (13 February 2015)

Fig. 8 presents the rates of the contribution of individual processes to the modeled sulfate concentrations in A1-A3 on 13–15 February 2015 and their diurnal variations. On 13 February, in the early stage of transport, sulfate concentrations were mainly distributed in A1. Because of a gradual decrease in upwind transport (i.e., aggregation of horizontal and vertical transport) from regions near the Shandong Peninsula, concentrations decreased until 09:00 LST ($-0.493 \mu g/m^3/h$)

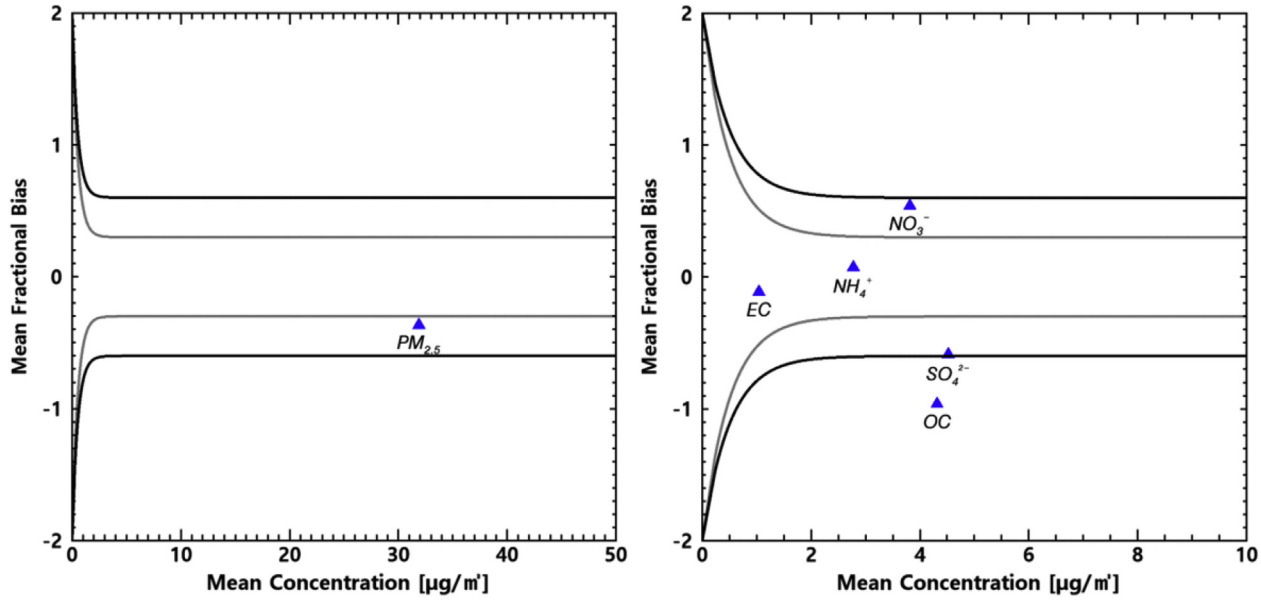


Fig. 4. Comparisons between the CMAQ-simulated and observed concentrations of $PM_{2.5}$ and its constituents at three measuring sites (Fig. 1) during the entire period of simulation (February 2015).

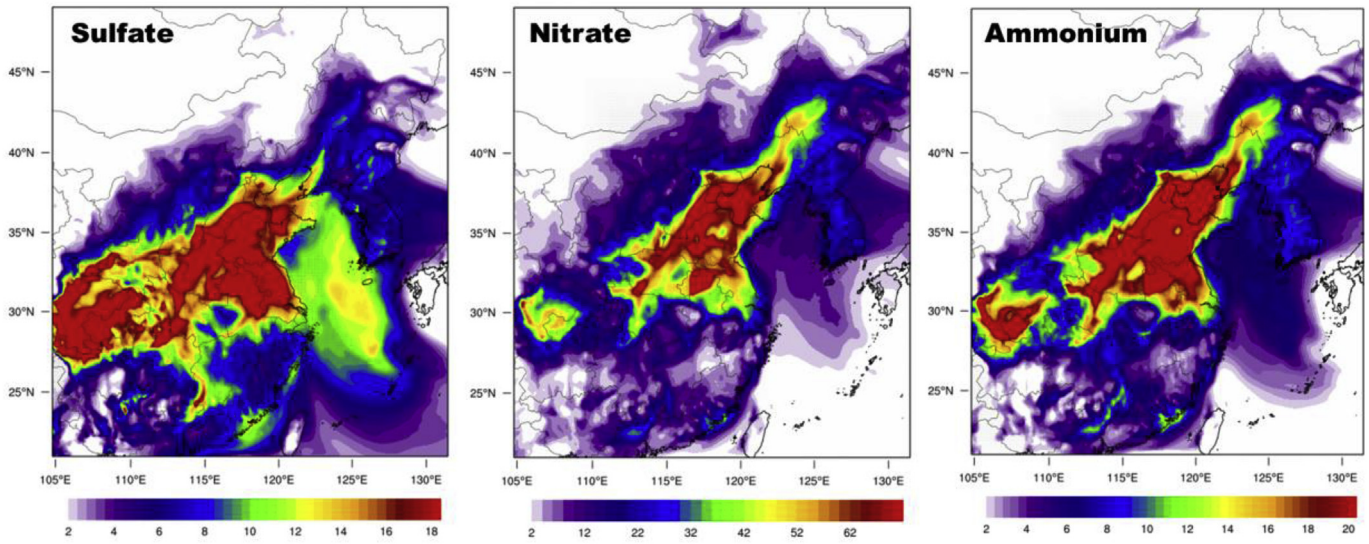


Fig. 5. Distributions of the CMAQ-simulated sulfate, nitrate, and ammonium concentrations over Eastern China and Korea. The values are averages in the PBL height during 13–15 February 2015.

and then began to increase in A1 around 09:00 LST. It should be noted that the increase was not due to upwind transport, but instead, to other processes. Fig. 8-(a) show that the sulfate concentration in A1 was affected by vertical transport (0.374–0.994μg/m^3/h), the aerosol process (i.e., gas-to-particle conversion and coagulation) (0–0.239μg/m^3/h), and horizontal transport (−1.688 to −0.200μg/m^3/h). These findings indicate that the increasing sulfate in A1 after 09:00 LST (0.373μg/m^3/h) was mostly due to sulfate production by the aerosol process and its vertical mixing resulting from momentum transport caused by vertical wind shear and temperature gradient. The chemically produced sulfate by aerosol process, particularly during the daytime, was vertically mixed and consequently led to the increased vertical transport rate of sulfate, attributable to the increase in sulfate concentration in A1. Table 2 lists all of the contributors to total sulfate productions in A1-A3 on 13–15 February 2015, calculated by the STM. The table shows that 82.31% of sulfate concentrations over the sea surface areas (A1-A3) were produced by the OH + SO_2 → H_2SO_4 + HO_2 reaction, implying that SO_2 oxidation by OH was a predominant contributor to sulfate production during its transport from the East China Sea to Korea. The transported SO_2 from upwind source regions (e.g., the Shandong Peninsula) reacted to abundant OH over the sea surface and formed sulfuric acid (H_2SO_4), which was then converted to sulfate (He et al., 2014). The contributions of the H_2O_2 + S(IV) → S(VI) + H_2O reaction (3.72%), sulfate emission transported from upwind source regions (6.59%), and other contributors (7.12%) (e.g., initial and boundary conditions) to total sulfate concentrations in A1-A3 were relatively minimal compared to that of the OH + SO_2 → H_2SO_4 + HO_2 reaction (82.31%). The significant contribution of Chinese SO_2 to sulfate production in downwind areas (e.g., the Yellow Sea and the Korea Strait) is consistent with findings by Itahashi et al. (2012).

The primary contributor to sulfate loss in A1 after 09:00 LST on 13 February was horizontal transport (Fig. 8-(a)). Sulfate was dispersed and deposited during its transport toward the downwind regions (the Yellow Sea and the Korea Strait) along with the prevailing southerly wind. These processes, however, did not cause the decrease in sulfate concentration because the total sulfate loss rate by horizontal transport and dry deposition was lower than the total production rate by the aerosol process and vertical transport. Consequently, the net rate of the sulfate change in A1 (09:00–24:00 LST) increased (from 0.012 to 0.555 μg/m^3/h), elevating the sulfate concentration in A1 on 13 February.

3.3.2. Sulfate changes in the middle stage of transport (14 February 2015)

In the middle stage of sulfate transport (14 February 2015), the high concentrations of sulfate were mainly distributed in A2 (Fig. 7). They continued to increase because of the combined effect of upwind transport and chemical production. Before the sun rose (00:00–09:00 LST), sulfate concentration in A2 increased (0.615μg/m^3/h) without chemical production by the aerosol process, attributable to the increased rate (from 0.291 to 0.866μg/m^3/h) of net transport (i.e., the aggregation of horizontal and vertical transport). It continued to increase until 12:00 LST, but kept almost same during the daytime (12:00–18:00 LST) despite the positive chemical production by the aerosol process (from 0 to 0.301μg/m^3/h). During the morning time (00:00–12:00 LST) on February 14, sulfate decrease by horizontal transport in A2 was minimal because of the wind flow in clockwise direction over A2 (Fig. 6), resulting in hovering of sulfate over A2. During the daytime (12:00–18:00 LST), however, northwestward wind blew over A2 and it resulted in strong horizontal transport of sulfate from A2 to the Shandong Peninsula. The negative horizontal transport contributed to the decrease in sulfate concentration in A2, canceling out the increase in sulfate by aerosol process and its vertical transport. The combined effect of them led to the nearly constant sulfate concentrations in A2 during the daytime. The decrease in sulfate concentration by negative horizontal transport was mitigated gradually as the wind direction in A2 turned to be north/northeastward after 18:00 LST, and the sulfate concentration in A2 increased again. After 19:00 LST, sulfate production by the aerosol process fell to nearly zero because of the absence of solar radiation, indicating that the increase in sulfate was solely affected by upwind transport. The sulfate concentration in A2 continued to increase and peaked (14.379μg/m^3) around midnight on 14 February.

3.3.3. Sulfate changes in the latter stage of transport (15 February 2015)

The IPR analysis results in the latter stage of sulfate transport (15 February 2015) (Fig. 8-(c)) indicated a clear difference from those on 13–14 February. At 00:00–09:00 LST, the sulfate concentration remained almost the same (≈13.496μg/m^3/h) due to balanced rates of positive upwind and negative downwind transport, but it began to decrease around 10:00 LST. The dramatic decrease was due to minimal sulfate production by the aerosol process (from 0 to 0.055μg/m^3/h) and significant loss by the cloud process (i.e., cloud attenuation of photolytic rates, mixing and scavenging by clouds, the chemistry of the aqueous phase, and wet deposition) (from −1.160 to −0.221μg/m^3/h).

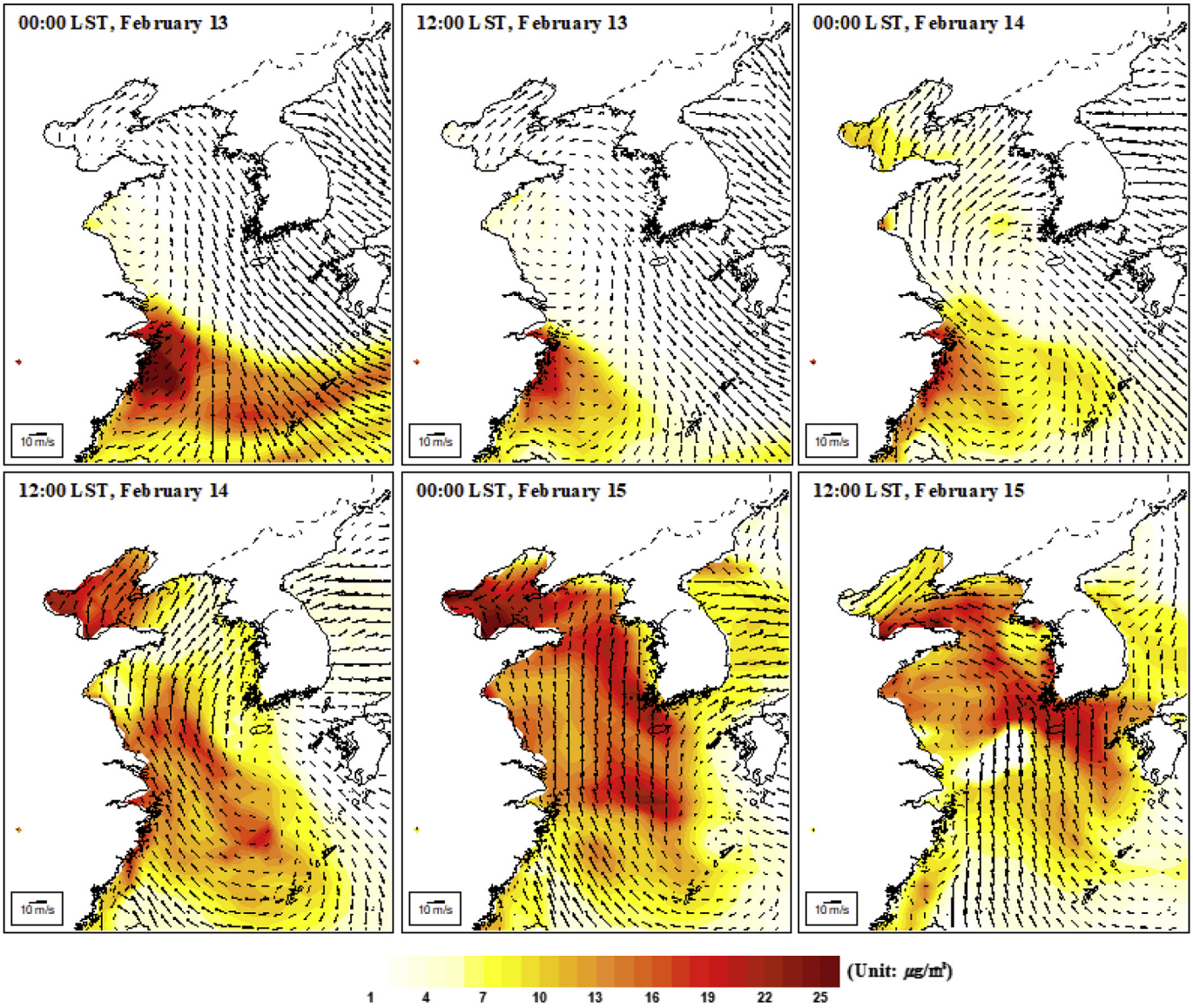


Fig. 6. Horizontal distributions of the CMAQ-simulated sulfate concentrations over the sea surface areas between Eastern China and Korea on 13–15 February. The values are averages in the PBL height.

The minimal chemical sulfate production in A3 on 15 February was likely due to the relatively low concentration of surplus SO_2 in the transporting PM plumes. Participating in chemical reactions associated with sulfate production, SO_2 concentrations gradually decreased during the transport from A1 to A3 (Table 3).

The significant sulfate loss by the cloud process on 15 February (from −1.160 to −0.221 μg/m^3/h) was distinguishable from that occurring on 13–14 February (0μg/m^3/h), attributable to the difference in meteorology. Fig. S6 and Table 4 illustrate synoptic weather patterns over Northeast Asia and observed meteorological factors in Korea on 15 February, which differed from those on 13–14 February. The observed cloud fraction on 15 February (82.28%) was much higher than the fractions on 13 (6.69%) and 14 February (32.43%). Corresponding to the high cloud fraction on 15 February, the amount of solar radiation was smaller than on 13 and 14 February. Moreover, relative humidity on 15 February (76.52%) was higher than on 13 (55.49%) and 14 February (75.84%) despite the relatively higher temperature, indicating that 15 February was relatively humid compared to 13 and 14 February. Because of the cloudy and humid meteorological conditions on 15 February, the sulfate loss rate by the cloud process (particularly wet scavenging) (from −1.160 to −0.221μg/m^3/h) was much higher than on 13–14 February (0μg/m^3/h), causing the steep decrease in sulfate in A3, which began around 10:00 LST on 15 February.

Another reason for the decreasing sulfate in A3 on 15 February, compared to the previous days, was the minimal sulfate production rate by the aerosol process (from 0 to 0.055μg/m^3/h), the result of the relatively lower SO_2 concentrations in A3 (1.62μg/m^3) than those in A1 and A2 (4.19 and 4.11μg/m^3, respectively). Since the surplus SO_2 in the transporting PM plumes was continuously used for sulfate production in A1-A2, its concentrations in A3 were smaller than those in A1-A2. As a result of the significant sulfate loss by the cloud process and minimal sulfate production by the aerosol process, sulfate concentration in A3 on February 15 began to decrease around 10:00 LST.

3.3.4. *Sulfate enhancement in Korea due to the transport*

Although the results from CMAQ simulation indicated a clear increase in sulfate on the sea surface areas (i.e., the East China Sea, Yellow Sea, Korea Strait), its impact on the enhanced sulfate in Korea need to be verified. Thus we analyzed the variations in the observed sulfate concentrations at three sites in Korea (i.e., Jeju, Ulasn, Seoul, and Baekyrongdo) on 13–15 February. The CMAQ-simulated sulfate concentrations did not perfectly match the corresponding observations,

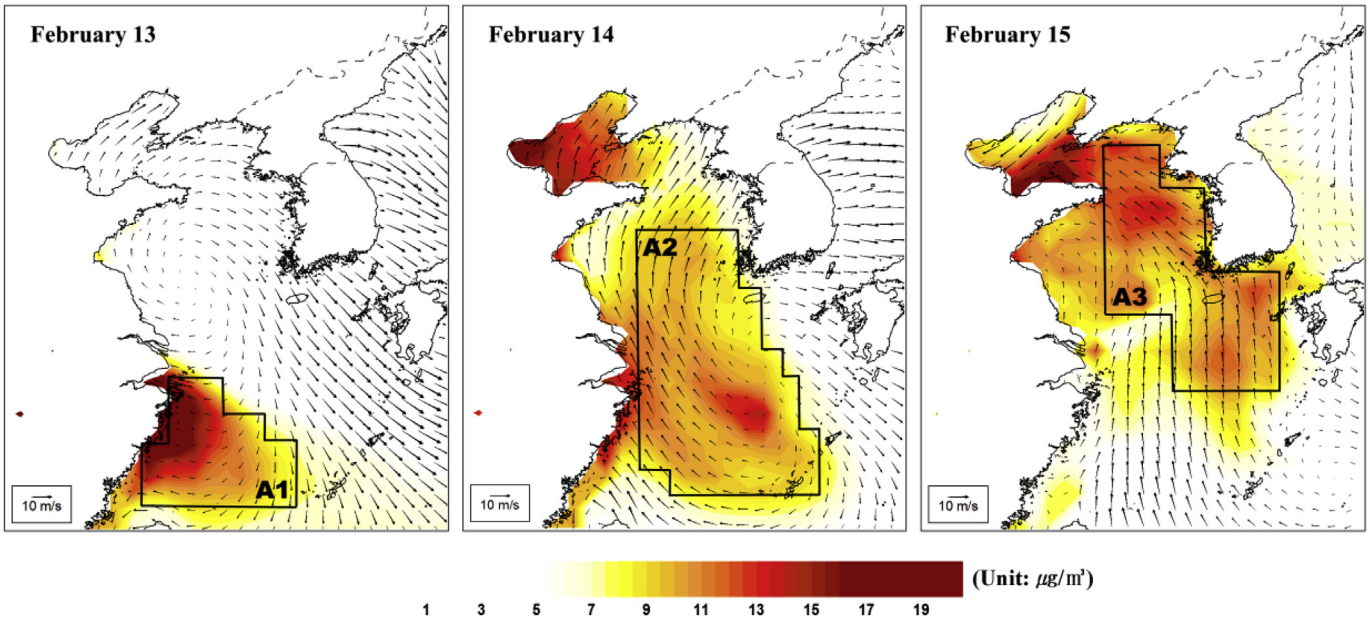


Fig. 7. Daily mean sulfate concentrations (in the PBL height) over the sea surface areas between Eastern China and Korea on 13–15 February. The three areas A1, A2, and A3 are the locations where the transporting sulfate remained on 13, 14, and 15 February, respectively.

attributable to uncertainties in emissions and meteorology, but reasonably reproduced their diurnal variations (Fig. S7). It implies that the model results based on IPR and STM analysis are reliable hence they can be used to interpret the variations in the observed sulfate concentrations at the three sites.

As shown in Fig. 9, the observed sulfate concentration at the Jeju site (Fig. 1) on 13 February was low (up to 1.81μg/m^3) with minimal variation, but began to increase around 00:00 LST on 14 February in response to arrival of upwind transport of sulfate from A1-A2. It increased gradually and peaked (13.07μg/m^3) around 22:00 LST, demonstrating that upwind transport was responsible for the sulfate enhancement in Jeju. It is important to note that the sulfate was not directly transported from source regions (e.g., Eastern China), but it was chemically produced primarily through SO_2 oxidation over the sea surface (A1-A2) during transport. The observed sulfate concentrations at the Ulsan and Baekryongdo sites (Fig. 1) show a clear increase on 15 February, implying that the enhanced sulfate over the sea surface areas (A1-A3) contributed to the high sulfate concentrations in Korea. The observed sulfate concentration in Ulsan reached a peak (13.74μg/m^3) around 18:00 LST on 15 February, which was later than in Jeju (22:00 LST on 14 February) because of the relatively late arrival of the upwind transport of sulfate from A1-A3. By the same token, the observed sulfate at the Baekryongdo site reached a peak (12.27μg/m^3) around 24:00 LST on 15 February, later than that it did at the Ulsan site. The observed sulfate data support the strong impact of upwind transport of sulfate on enhancement in the observed sulfate concentrations in Korea, but the respective contributions of local production and upwind transport to the enhanced sulfate still remain unclear. Therefore, it need to be clarified by conducting several sensitivity simulations based on Brute Force Method (BFM) and/or Decoupled Direct Method (DDM) in the future study.

3.4. Sensitivity of increasing sulfate to meteorology

As demonstrated in the previous sections, sulfate production on the sea surface during its transport from Eastern China to Korea dominantly occurred under the clear weather condition (13–14 February). However, it remains unclear which meteorological factor is the most important for the sulfate production. Hence we conducted several sensitivity simulations on 13–14 February with increased temperature (5 °C: TEMP_5D, 10 °C: TEMP_10D), cloud fraction (10%: CFRAC_10P, 20%: CFRAC_20P), and the water vapor mixing ratio (10%: QV_10P, 20%: QV_20P) to quantitatively investigate the sensitivity of sulfate production/loss to the variations in meteorology.

Table 5 summarizes the results of each sensitivity run. It shows that the sulfate production rate by an aerosol process in A1-A2 on 13–14 February was proportional to increases in the temperature. The sulfate production rate resulting from the aerosol process increased by roughly 0.006μg/m^3/h in response to a temperature increase of 5 °C. This increase was likely due to more activated SO_2 oxidation in A1-A2 corresponding to the increased temperature. The impact of the increased cloud fraction led to negligible changes in sulfate production/loss rates, consistent with the results presented in a previous study (Liu et al., 2011). The increased water vapor mixing ratio resulted in increased production rates by the cloud process (0.026μg/m^3/h per 10%); however, this finding is not easy to be explained because of the complexity and non-linearity in the aqueous phase chemistry of sulfate linked to those of other species (e.g., ammonium and nitrate) (Binkowsky and Roselle, 2003; Liu et al., 2011; Huang et al., 2014; Li et al., 2014; Lin et al., 2017).

Those results implies that temperature is the most important meteorological factor affecting the sulfate production on the sea surface during its transport from Eastern China to Korea. It suggests that each transport event with the same pathway could differently affect the sulfate concentrations in downwind regions, depending on meteorological conditions, particularly temperature. Validation of these findings, however, requires more sensitivity testing and detailed analyses.

4. Summary and conclusions

This study investigated changes in the concentrations of sulfate over sea surface areas during its transport from Eastern China and Korea. We used CMAQ to simulate sulfate concentrations over Northeast Asia in February 2015. Results of the evaluation indicated the reasonable accuracy of simulated concentrations of $PM_{2.5}$ and its constituents with high IOA values (from 0.63 to 0.85) and low biases (from −4.30 to 4.84 μg/m^3). To examine the behavior of sulfate during transport in detail, we selected a partial period (13–15 February 2015) in which long-range transport of highly polluted air from Eastern China to Korea occurred. On 13–15 February, compared to simulated nitrate and ammonium, the

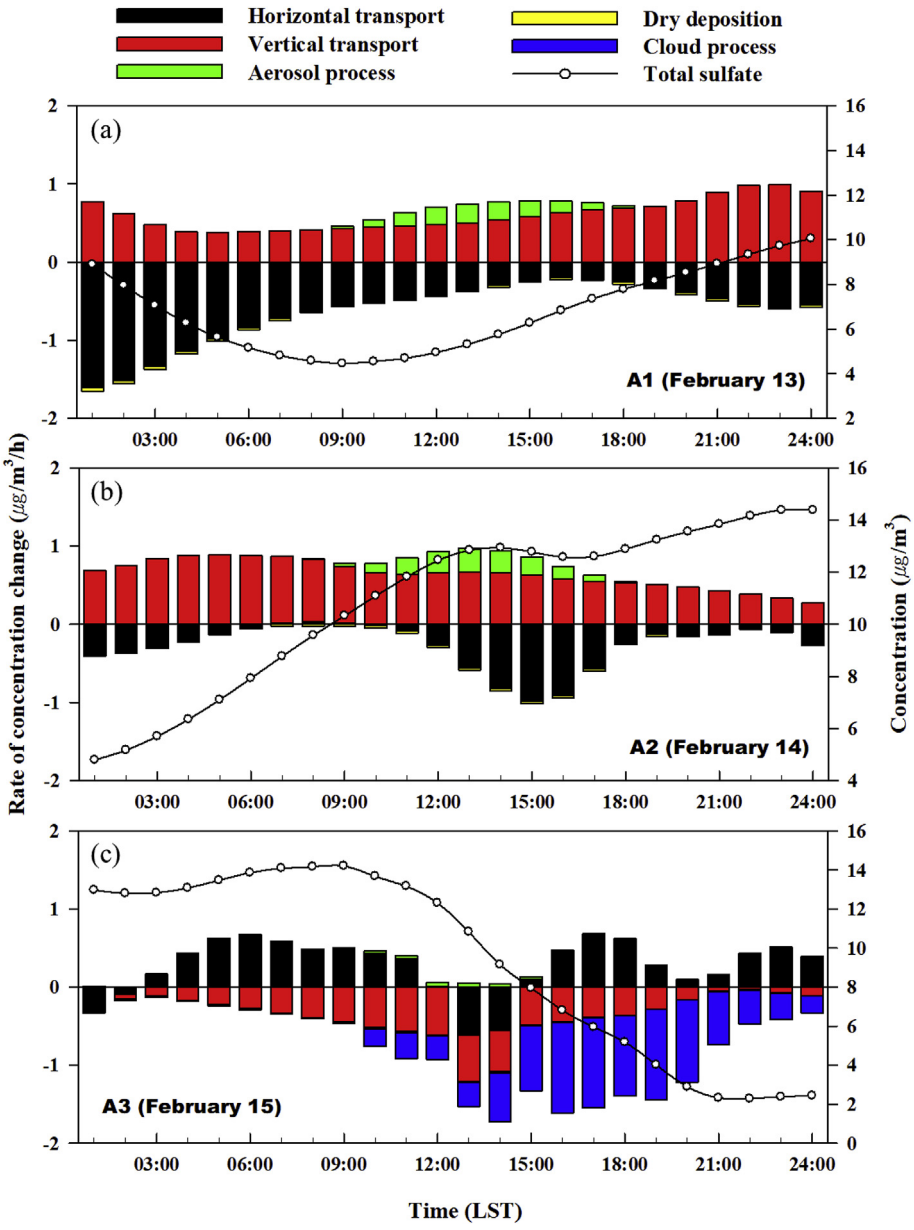


Fig. 8. Diurnal variations of the contribution rates of each process to modeled sulfate concentrations in (a)–(c) A1-A3 on 13–15 February 2015.

Table 2
Contributions (%) of individual chemical reactions, emissions, and other factors to total sulfate productions in A1-A3 on 13–15 February. The values are averages in the PBL height.

	A1 (%)	A2 (%)	A3 (%)	A1-A3 (%)
$OH + SO_2 \rightarrow H_2SO_4 + HO_2$	82.11	84.24	80.57	82.31
$H_2O_2 + S(IV) \rightarrow S(VI) + H_2O$	0.88	2.50	7.78	3.72
$O_3 + S(IV) \rightarrow S(VI) + O_2$	0.01	0.01	0.20	0.07
$O_2 + S(IV) \rightarrow S(VI)$	0.06	0.10	0.13	0.10
MHP + S(IV) → S(VI)	0.01	0.01	0.04	0.02
PAA + S(IV) → S(VI)	0.02	0.05	0.14	0.07
Emissions	8.64	6.43	4.70	6.59
Others	8.28	6.66	6.44	7.12

simulated sulfate featured a distinct spatial distribution, indicating high concentrations near the western part of the East China Sea (A1) on 13 February, the central/southern parts of the Yellow Sea (A2) on 14 February, and the northern/eastern parts of the Yellow Sea and the Korea Strait (A3) on 15 February. Interestingly, despite nearly zero

Table 3
The CMAQ-simulated mean SO_2 concentrations (μg/m^3) in A1-A3 on 13–15 February 2015. The values are averages in the PBL height.

	A1 (13 Feb)	A2 (14 Feb)	A3 (15 Feb)
SO_2 concentration (μg/m$_3$)	4.19	4.11	1.62

Table 4
Observed meteorological factors obtained from ASOS data on 13–15 February 2015. The values are the averages of 18 coastal sites located in the western and southern regions of Korea, which face the Yellow Sea and the Korea Strait.

	13 February	14 February	15 February
Cloud fraction (%)	6.69	33.43	82.28
Solar radiation (Wh^{-1}m^2)	323.61	224.13	109.03
Temperature (°C)	−1.18	2.10	7.48
Wind speed (ms^{-1})	2.60	2.04	2.64
Relative humidity (%)	55.49	75.84	76.52

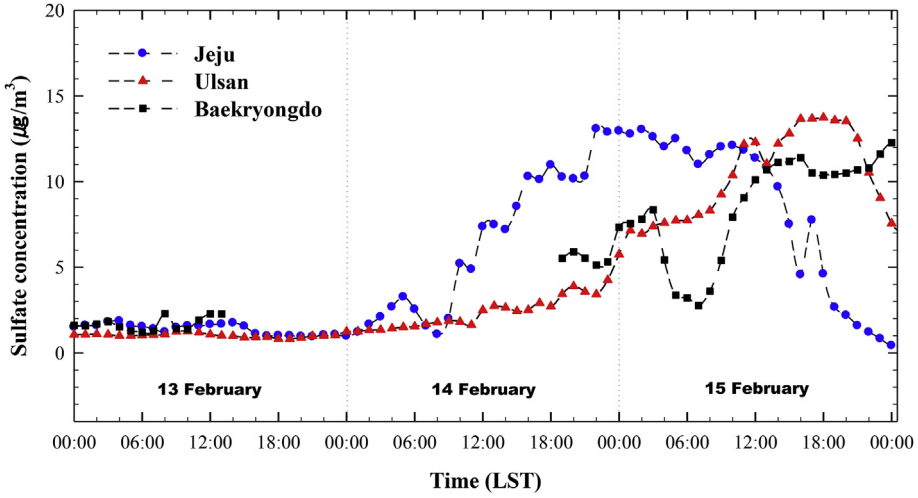


Fig. 9. Time series of observed sulfate concentrations on 13–15 February 2015 at three measuring sites in Korea (Fig. 1).

Table 5
The simulated sulfate production/loss rates (μg/m^3/h) by aerosol and cloud processes in A1-A2 on 13–14 February from the respective CMAQ sensitivity simulations. The values are averages in the PBL height.

	13–14 February (A1-A2)	
	Aerosol process	Cloud process
Base	0.038	0.006
TEMP_5D	0.043	0.000
TEMP_10D	0.050	0.000
CFRAC_10P	0.038	0.006
CFRAC_20P	0.038	0.006
QV_10P	0.037	0.052
QV_20P	0.035	0.058

anthropogenic emissions in these areas, the concentrations of sulfate gradually increased while it passed over sea surface areas (A1-A3).

To further investigate the increasing amount of sulfate on the sea surface, we conducted a quantitative analysis using the IPR module in CMAQ. It indicated that the aerosol process and vertical transport played a crucial role in increasing concentrations of sulfate over the sea surface during transport. In the early (13 February) and middle (14 February) stages of sulfate transport, concentrations continued to increase. We attribute the sustaining increase in sulfate to the chemical production of sulfate by the aerosol process (up to 0.866μg/m^3/h) and vertical transport (up to 0.994μg/m^3/h), particularly during the daytime. Results from STM simulations indicated that the $OH + SO_2 \rightarrow H_2SO_4 + HO_2$ reaction was the largest contributor (82.31%) to the production of sulfate over the sea surface areas (A1-A3) during its transport, implying that the increased concentrations of sulfate primarily resulted from SO_2 oxidation by OH. Surplus SO_2 in the transporting plume reacted to abundant OH over the sea surface and formed H_2SO_4, which was converted to sulfate, the primary reason for the increasing concentrations of sulfate during its transport from Eastern China to Korea. The increase in sulfate concentrations during the transport, however, was not sustained in the latter stage of transport (15 February). On 15 February, the net rate of change in the sulfate was negative because of predominant sulfate loss by cloud scavenging, attributable to cloudy and humid meteorological conditions. Moreover, sulfate production by the aerosol process on 15 February, compared to that on 13–14 February, was relatively minimal. The significant cloud scavenging and minimal chemical production led to a decrease in sulfate concentrations on 15 February. Observed sulfate concentrations at three measuring sites in Korea (Jeju, Ulsan, and Baekryongdo) exhibited dramatic increases in sulfate concentrations on 14–15 February. These findings indicate that sulfate over the sea surface areas between the East China Sea and Korea enhanced sulfate concentrations in Korea (12.27–13.74μg/m^3). It should be noted, however, that sulfate was not directly transported from upwind regions, but it was chemically produced during transport.

The results generated by several sensitivity simulations with varied meteorology revealed that chemical sulfate production/loss rates during transport from Eastern China to Korea depend on meteorological conditions, particularly temperature. These results, along with those above, identify the mechanism of increasing concentrations of sulfate during its transport from Eastern China to Korea and its impact on high sulfate concentrations in Korea. However, further case studies that analyze other time periods using updated emissions and large-scale observations (e.g., remote sensing and aircraft measurements) need to be conducted for the better model evaluations, making those results more reliable. They will be helpful to verify the exact mechanisms of high PM events in the downwind regions of pollutants sources, particularly in Korea.

Acknowledgements

This subjec is supported by Korea Ministry of Environment (MOE) as “the Chemical Accident Prevention Technology Development Project” (No. 2015001950002).

Appendix A. Supplementary data

Supplementary data related to this article can be found at http://dx.doi.org/10.1016/j.atmosenv.2018.05.017.

References

Boylan, J.W., Russell, A.G., 2006. PM and light extinction model performance metrics, goals, and criteria for three-dimensional air quality models. Atmos. Environ. 40, 4946–4959.

Binkowsky, F.S., Roselle, S.J., 2003. Models-3 community multiscale air quality (CMAQ) model aerosol component 1. Model description. J. Geophys. Res. 108, 4183. http://dx.doi.org/10.1029/2001JD001409.

Byun, D., Schere, K.L., 2006. Review of the governing equations, computational algorithms, and other components of the Models-3 Community Multiscale Air Quality (CMAQ) modeling system. Appl. Mech. Rev. 59, 51–77.

Chang, L.-S., Cho, A., Park, H., Nam, K., Kim, D., Hong, J.-H., Song, C.-K., 2016. Human-model hybrid Korean air quality forecasting system. J. Air Waste Manag. Assoc. 66, 896–911.

Choi, J.-K., Heo, J.-B., Ban, S.-J., Yi, S.-M., Zoh, K.-D., 2013. Source apportionment of $PM_{2.5}$ at the coastal area in Korea. Sci. Total Environ. 447, 370–380.

Choi, K.-C., et al., 2014. Assessment of transboundary ozone contribution toward South Korea using multiple source-receptor modeling techniques. Atmos. Environ. 92, 118–129.

Fan, Q., et al., 2015. Process analysis of regional aerosol pollution during spring in the Pearl River Delta region, China. Atmos. Environ. 122, 829–838.
Ghim, Y.S., Choi, Y., Kim, S., Bae, C.H., Park, J., Shin, H.J., 2017. Evaluation of model performance for forecasting fine particle concentrations in Korea. Aerosol Air Qual. Res. 17, 1856–1864.
Gipson, G.L., Young, J., 1999. Process Analysis. Science Algorithms of the EPA Models-3 Community Multiscale Air Quality (CMAQ) Modeling System. Available at: https://www.cmascenter.org/cmaq/science_documentation/pdf/ch16.pdf.
Guenther, A.B., Jiang, X., Heald, C.L., Sakulyanontvittaya, T., Duhl, T., Emmons, L.K., Wang, X., 2012. The model of emissions of gases and aerosols from nature version 2.1 (MEGAN2.1): an extended and updated framework for modeling biogenic emissions. Geosci. Model Dev. 5, 1471–1492.
Han, J.S., Moon, K.J., Kong, B.J., Lee, S.J., Kim, J.E., Kim, Y.J., 2005. Seasonal variation of chemical composition in fine particles at Gosan, Korea. Environ. Monit. Assess. 107, 221–237.
Han, J.S., Moon, K.J., Kim, Y.J., 2006. Identification of potential sources and source regions of fine ambient particles measured at Gosan background site in Korea using advanced hybrid receptor model combined with positive matrix factorization. J. Geophys. Res. 111, D22217.
He, H., Wang, Y., Ma, Q., Chu, B., Ji, D., Tang, G., Liu, C., Zhang, H., Hao, J., 2014. Mineral dust and NO_x promote the conversion of SO_2 to sulfate in heavy pollution days. Sci. Rep. 4, 4172.
Heo, J.-B., Hopke, P.K., Yi, S.-M., 2009. Source apportionment of $PM_{2.5}$ in Seoul, Korea. Atmos. Chem. Phys. 9, 4957–4971.
Huang, X., Song, Y., Zhao, C., Li, M., Zhu, T., Zhang, Q., Zhang, X., 2014. Pathways of sulfate enhancement by natural and anthropogenic mineral aerosols in China. J. Geophys. Res. Atmos. 119, 14165–14179.
Itahashi, S., Uno, I., Kim, S., 2012. Source contributions of sulfate aerosol over East Asia estimated by CMAQ-DDM. Environ. Sci. Technol. 46 (12), 6733–6741.
Itahashi, S., Yumimoto, K., Uno, I., Hayami, H., Fujita, S.-i., Pan, Y., Wang, Y., 2018. A 15-year record (2001–2015) of the ratio of nitrate to non-sea-salt sulfate in precipitation over East Asia. Atmos. Chem. Phys. 18, 2835–2852.
Jeon, W.-B., Lee, S.-H., Lee, H.-W., Kim, H.-G., 2012. Process analysis of the impact of atmospheric recirculation on consecutive high-O_3 episodes over the Seoul Metropolitan area in the Korean Peninsula. Atmos. Environ. 63, 213–222.
Jeon, W.-B., Lee, H.W., Lee, S.-H., Park, J.-H., Kim, H.-G., 2014a. Numerical study on the characteristics of high $PM_{2.5}$ episodes in Anmyeondo area in 2009. J. Environ. Sci. Int. 23 (2), 249–259.
Jeon, W.-B., Lee, S.-H., Lee, H., Park, C., Kim, D.-H., Park, S.-Y., 2014b. A study on high ozone formation mechanism associated with change of NO_x/VOCs at a rural area in the Korean Peninsula. Atmos. Environ. 89, 10–21.
Jeon, W., Choi, Y., Lee, H.W., Lee, S.-H., Yoo, J.-W., Park, J., Lee, H.-J., 2015. A quantitative analysis of grid nudging effect on each process of $PM_{2.5}$ production in the Korean Peninsula. Atmos. Environ. 122, 763–774.
Jeon, W., Choi, Y., Percell, P., Souri, A.H., Song, C.-K., Kim, S.-T., Kim, J., 2016. Computationally efficient air quality forecasting tool: implementation of STOPS v1.5 model into CMAQ v5.0.2 for a prediction of Asian dust. Geosci. Model Dev. 9, 3671–3684.
Jeon, W., Choi, Y., Souri, A.H., Roy, A., Diao, L., Pan, S., Lee, H.W., Lee, S.-H., 2018. Identification of chemical fingerprints in long-range transport of burning induced upper tropospheric ozone from Colorado to the North Atlantic Ocean. Sci. Total Environ. 613–614, 820–828.
Kim, B.-U., Kim, O., Kim, H.C., Kim, S., 2016. Influence of Fossil-fuel Power Plant Emissions on the Surface Fine Particulate Matter in the Seoul Capital Area, South Korea.
Kim, B.-U., Bae, C., Kim, H.C., Kim, E., Kim, S., 2017b. Spatially and chemically resolved source apportionment analysis: case study of high particulate matter event. Atmos. Environ. 162, 55–70.
Kim, H.C., Kim, E., Bae, C., Cho, J.H., Kim, B.-U., Kim, S., 2017a. Regional contributions to particulate matter concentration in the Seoul metropolitan area, South Korea: seasonal variation and sensitivity to meteorology and emissions inventory. Atmos. Chem. Phys. 17, 10315–10332.
Kim, S.-W., Yoon, S.-C., Kim, J., Kang, J.-Y., Sugimoto, N., 2010. Asian dust event observed in Seoul, Korea, during 29-31 May 2008: analysis of transport and vertical distribution of dust particles from lidar and surface measurements. Sci. Total Environ. 408, 1707–1718 J. Air Waste Manag. Assoc. 66(9), 863–873.
Krotkov, N.A., McLinden, C.A., Li, C., Lamsal, L.N., Celarier, E.A., Marchenko, S.V., Swartz, W.H., Bucsela, E.J., Joiner, J., Duncan, B.N., Boersma, K.F., Veefkind, J.P., Levelt, P.F., Fioletov, V.E., Dickerson, R.R., He, H., Lu, Z., Streets, D.G., 2016. Aura OMI observations of regional SO_2 and NO_2 pollution changes from 2005 to 2015. Atmos. Chem. Phys. 16, 4605–4629.
Li, L., Huang, C., Huang, H.Y., Wang, Y.J., Yan, R.S., Zhang, G.F., Zhou, M., Lou, R.S., Tao, S.K., Wang, H.L., Qiao, L.P., Chen, C.H., Streets, D.G., Fu, J.S., 2014. An integrated process rate analysis of a regional fine particulate matter episode over Yangtze River Delta in 2010. Atmos. Environ. 91, 60–70.
Li, M., Zhang, Q., Kurokawa, J.-i, Woo, J.-H., He, K., Lu, Z., Ohara, T., Song, Y., Streets, D.G., Carmichael, G.R., Cheng, Y., Hong, C., Huo, H., Jiang, X., Kang, S., Liu, F., Su, H., Zheng, B., 2017. MIX: a mosaic Asian anthropogenic emission inventory for the MICS-Asia and the HTAP projects. Atmos. Chem. Phys. 17, 935–963.
Lin, M., Biglari, S., Zhang, Z., Crocker, D., Tao, J., Su, B., Liu, L., Thiemens, M.H., 2017. Vertically uniform formation pathways of tropospheric sulfate aerosols in East China detected from triple stable oxygen and radiogenic sulfur isotopes. Geophys. Res. Lett. 44, 5187–5196.
Liu, P., Zhang, Y., Yu, S., Schere, K.L., 2011. Use of a process analysis tool for diagnostic study on fine particulate matter predictions in the U.S.-Part II: analyses and sensitivity simulations. Atmos. Pollut. Res. 2, 661–671.
Nolte, C.G., Appel, K.W., Kelly, J.T., Bhave, P.V., Fahey, K.M., Collett Jr., J.L., Zhang, L., Young, J.O., 2015. Evaluation of the Community Multiscale Air Quality (CMAQ) model v5.0 against size-resolved measurements of inorganic particle composition across sites in North America. Geosci. Model Dev. 8, 2877–2892.
Pan, S., Choi, Y., Roy, A., Li, X., Jeon, W., Souri, A.H., 2015. Modeling the uncertainty of several VOC and its impact on simulated VOC and ozone in Houston, Texas. Atmos. Environ. 120, 404–416.
Pan, S., Choi, Y., Roy, A., Jeon, W., 2017. Allocating emissions to 4 km and 1 km horizontal spatial resolutions and its impact on simulated NO_x and O_3 in Houston, TX. Atmos. Environ. 164, 398–415.
Park, R.J., Kim, S.W., 2014. Air quality modeling in East Asia: present issues and future directions. Asia-Pac. J. Atmos. Sci. 50, 105–120.
Park, S.-S., Cho, S.-Y., Jung, C.-H., Lee, K.-H., 2016. Characteristics of water-soluble inorganic species in PM_{10} and $PM_{2.5}$ at two coastal sites during spring in Korea. Atmos. Pollut. Res. 7, 370–383.
Paulot, F., Fan, S., Horowitz, L.W., 2017. Contrasting seasonal responses of sulfate aerosols to declining SO_2 emissions in the Eastern U.S.: implications for the efficacy of SO_2 emission controls. Geophys. Res. Lett. 44, 455–464.
Seinfeld, J.H., Pandis, S.N., 2006. Atmospheric Chemistry and Physics: from Air Pollution to Climate Change, second ed. John Wiley, New York.
Shin, H.J., Park, S.-M., Park, J.S., Song, I.H., Hong, Y.D., 2016. Chemical characteristics of high PM episodes occurring in Spring 2014, Seoul, Korea. Advances in Meteorology 2016, 2424875. http://dx.doi.org/10.1155/2016/2424875. 11 pages.
Son, J.-Y., Lee, J.-T., Kim, K.-H., Jung, K., Bell, M.L., 2012. Characterization of fine particulate matter and associations between particulate chemical constituents and mortality in Seoul, Korea. Environ. Health Perspect. 120, 872–878.
Souri, A.H., Choi, Y., Jeon, W., Woo, J.-H., Zhang, Q., Kurokawa, J.-i., 2017. Remote sensing evidence of decadal changes in major tropospheric ozone precursors over East Asia. J. Geophys. Res. Atmos. 122. http://dx.doi.org/10.1002/2016JD025663.
Skamarock, W., Klemp, J.B., Dudhia, J., Gill, D.O., Barker, D.M., Duda, M.G., Huang, X.-Y., Wang, W., Powers, J.G., 2008. A Description of the Advanced Research WRF Version 3. NCAR Technical Note, NCAR/TN/u2013475.
van der A, R.J., Mijling, B., Ding, J., Koukouli, M.E., Liu, F., Li, Q., Mao, H., Theys, N., 2017. Cleaning up the air: effectiveness of air quality policy for SO_2 and NO_x emissions in China. Atmos. Chem. Phys. 17, 1775–1789.
Yarwood, G., Rao, S., Yocke, M., Whitten, G., 2005. Updates to the Carbon Bond Chemical Mechanism: CB05. Final report to the US EPA, RT-0400675, available at: http://www.camx.com/publ/pdfs/cb05_final_report_120805.pdf, Accessed date: 13 July 2017.
Zhang, H., Li, J., Ying, Q., Yu, J.Z., Wu, D., Cheng, Y., He, K., Jiang, J., 2012. Source apportionment of $PM_{2.5}$ nitrate and sulfate in China using a source-oriented chemical transport model. Atmos. Environ. 62, 228–242.